Supporting Information:

Construction of Oxygen Vacancies-Enriched Triple Perovskite Oxide Electrocatalyst for Efficient and Stable Oxygen Evolution in Acidic Media

Yuanyuan Wu [a], Tixuan Xia [b], Lu Yang[a], Feifan Guo[c], Wei Jiang[b], Jihui Lang[d], Yunchao Ma [a], Jingdong Feng [a], Guangbo Che[e], Chunbo Liu[b*]*

[a] Key Laboratory of Preparation Application of Environmental Friendly Materials, Ministry of Education, College of Chemistry, Jilin Normal University, Siping 136000, P. R. China

[b] Jilin Joint Technology Innovation Laboratory of Developing and Utilizing Materials of Reducing Pollution and Carbon Emissions, College of Engineering, Jilin Normal University, Siping, 136000, P. R. China.

[c] Key Laboratory of Polyoxometalate and Reticular Material Chemistry of Ministry of Education, Faculty of Chemistry, Northeast Normal University, Changchun, 130024, China

[d] Key Laboratory of Functional Materials Physics and Chemistry of the Ministry of Education, Jilin Normal University, Changchun, 130103, China

[e] College of Chemistry, Baicheng Normal University, Baicheng, 13700, P. R. China

* *Corresponding author: Guangbo Che (*guangboche@jlnu.edu.cn*); Chunbo Liu (*chunboliu@jlnu.edu.cn*)*

1. Experimental Section

1.1 Chemicals and Reagents

Potassium hexachloroiridate(IV) (K_2IrCl_6, 99.99%) and ruthenium(IV) oxide (RuO_2, 99%) were purchased from Aladdin. Ruthenium chloride hydrate ($RuCl_3 \cdot xH_2O$, 99%), citric acid ($C_6H_8O_7$), Nafion® perfluorinated resin solution, strontium acetate ($C_4H_6O_4Sr$) and isopropyl alcohol ($(CH_3)_2CHOH$) were purchased from Shanghai Macklin Biochemical Co., Ltd. Ethylene glycol ($(CH_2OH)_2$) were purchased from Beijing Chemical Factory. Hydrochloric acid (HCl), Sulfuric acid (H_2SO_4) and ethanol absolute (C_2H_6O) was purchased from Sinopharm Chemical.

1.2 Material Characterizations

The powder X-ray diffraction (XRD) patterns were conducted by a Rigaku D/Max 2550 Xray diffractometer with Cu Kα radiation (λ = 1.5418 Å). The scanning electron microscope (SEM) images were obtained with a Regulus 8100 electron microscope. The transmission electron microscope (TEM) images and high-resolution transmission electron microscopy (HRTEM) images were carried out with a JEM-2100F transmission electron microscope. Energy dispersive X-ray (EDX) analysis was obtained with an EDX system attached to X-MaxN 80T transmission electron microscope (TEM). The XPS measurements were carried out on an ESCALAB 250Xi spectrometer (Thermo Scientific, USA) equipped with a pass energy of 30 eV with a power of 100 W (10 kV and 10 mA) and a mono-chromatized AlKα X-ray (h_v=1486.65 eV) source. All samples were analyzed under a pressure of less than $1.0\times10^{\wedge-9}$ Pa.

Spectra were acquired through the avantage software (Version 5.979) with a step of 0.05 eV.

1.3 DFT calculations

All the DFT calculations were conducted based on the Vienna Ab-inito Simulation Package (VASP) [1-2]. The exchange-correlation effects were described by the Perdew-Burke-Ernzerhof (PBE) functional within the generalized gradient approximation (GGA) method [3-4]. The core-valence interactions were accounted by the projected augmented wave (PAW) method [5]. The energy cutoff for plane wave expansions was set to 450 eV, and the 2×2×1 Monkhorst-Pack grid k-points were selected to sample the Brillouin zone integration. The vacuum space is adopted 15 Å above the surfaces to avoid periodic interactions. The structural optimization was completed for energy and force convergence set at 1.0×10^{-4} eV and 0.02 eV $Å^{-1}$, respectively.

The OER calaulation in acidic medium includes four-electron transfer procedure, and each reaction step as follows:

$$H_2O\ (l) + * \rightarrow OH* + H^+ + e^-$$

$$OH* \rightarrow O* + H^+ + e^-$$

$$O* + H_2O\ (l) \rightarrow OOH* + H^+ + e^-$$

$$OOH* \rightarrow O_2\ (g) + H^+ + e^-$$

where * refers to adsorption site of catalyst and *OOH, *O, *OH represent the reaction oxygen intermediates. The Gibbs free energy change (ΔG) of each step is calculated using the following formula:

$$\Delta G = \Delta E + \Delta ZPE - T\Delta S$$

where ΔE is the electronic energy difference directly obtained from DFT calculations, ΔZPE is the zero point energy difference, T is the room temperature (298.15 K) and ΔS is the entropy change. ZPE could be obtained after frequency calculation by [6]:

$$ZPE = \frac{1}{2}\sum hvi$$

And the TS values of adsorbed species are calculated according to the vibrational frequencies[7]:

$$TS = k_B T \left[\sum_k ln(\frac{1}{1 - e^{-hv/k_B T}}) + \sum_k \frac{hv}{k_B T} \frac{1}{(e^{hv/k_B T} - 1)} + 1 \right]$$

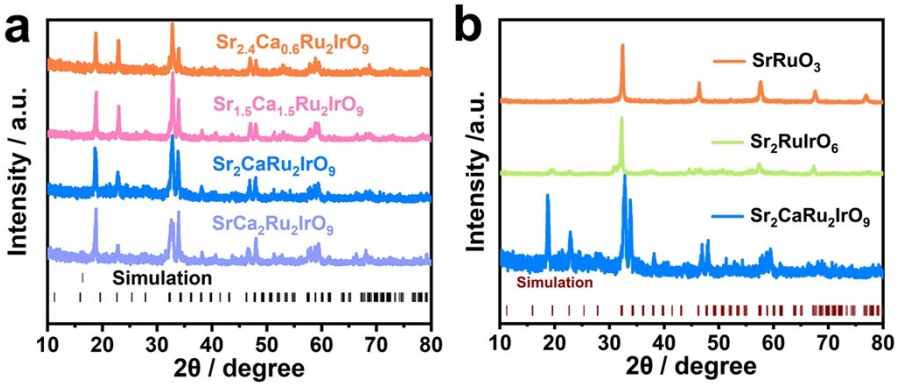

Fig. S1. X-ray diffraction (XRD) of (a) $Sr_xCa_{1-x}Ru_2IrO_9$ with different Sr: Ca atomic ratios and (b) $SrRuO_3$, Sr_2RuIrO_6, $Sr_2CaRu_2IrO_9$ and Simulated double perovskite.

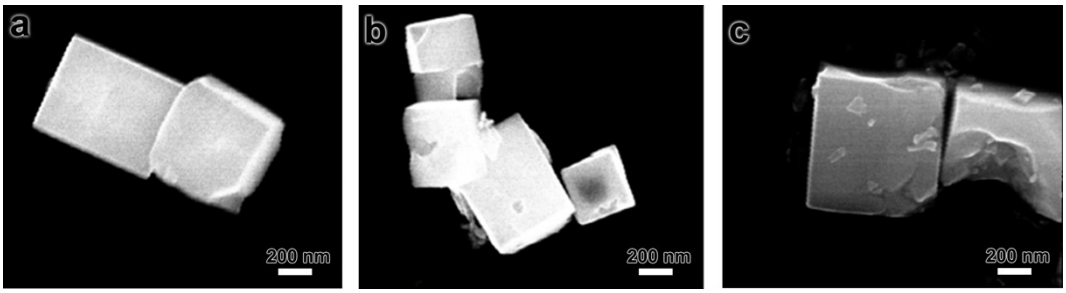

Fig. S2. (a-c) Scanning electron microscopy (SEM) of $Sr_{2.4}Ca_{0.6}Ru_2IrO_9$, $Sr_{1.5}Ca_{1.5}Ru_2IrO_9$ and $SrCa_2Ru_2IrO_9$.

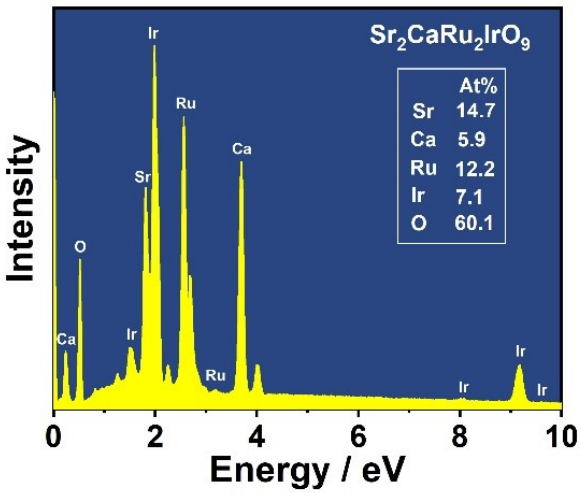

Fig. S3. Energy dispersive X-ray spectroscopy (EDX) of $Sr_2CaRu_2IrO_9$

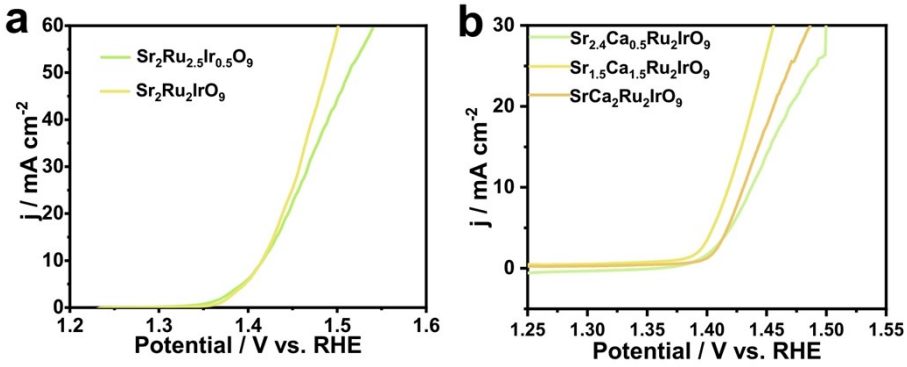

Fig. S4. (a) LSV curves of $Sr_2Ru_{2.5}Ir_{0.5}O_9$ and $Sr_2Ru_2IrO_9$. (b) LSV curves of $Sr_xCa_{1-x}Ru_2IrO_9$ with different Sr: Ca atomic ratios.

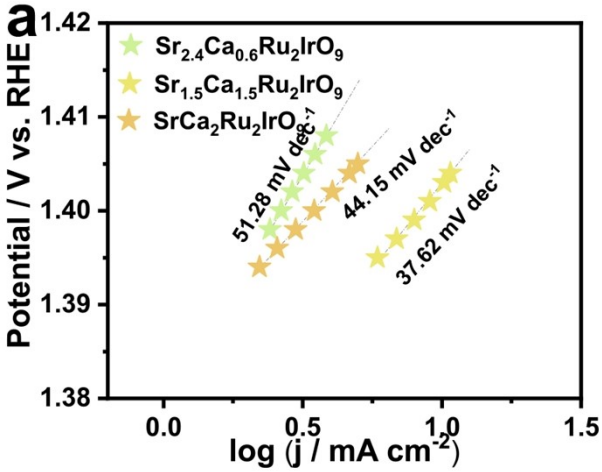

Fig. S5. Tafel slope of $Sr_xCa_{1-x}Ru_2IrO_9$ with different Sr: Ca atomic ratios.

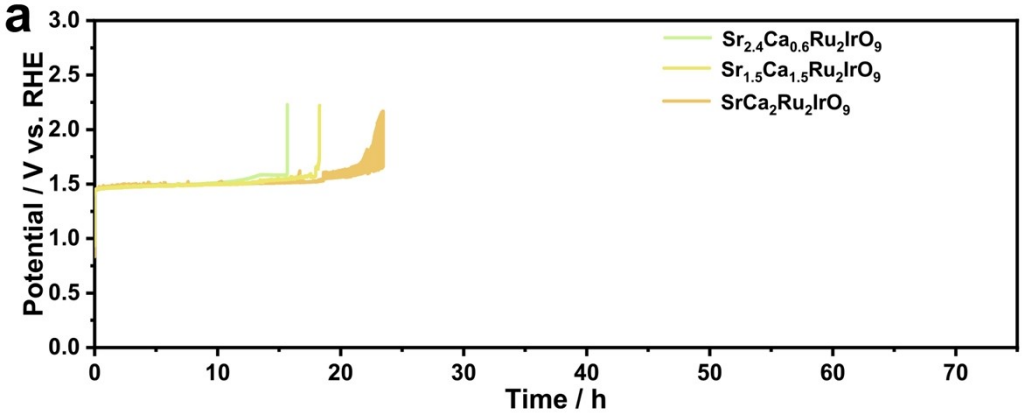

Fig. S6. Chronopotentiometry curve of $Sr_xCa_{1-x}Ru_2IrO_9$ with different Sr: Ca atomic ratios.

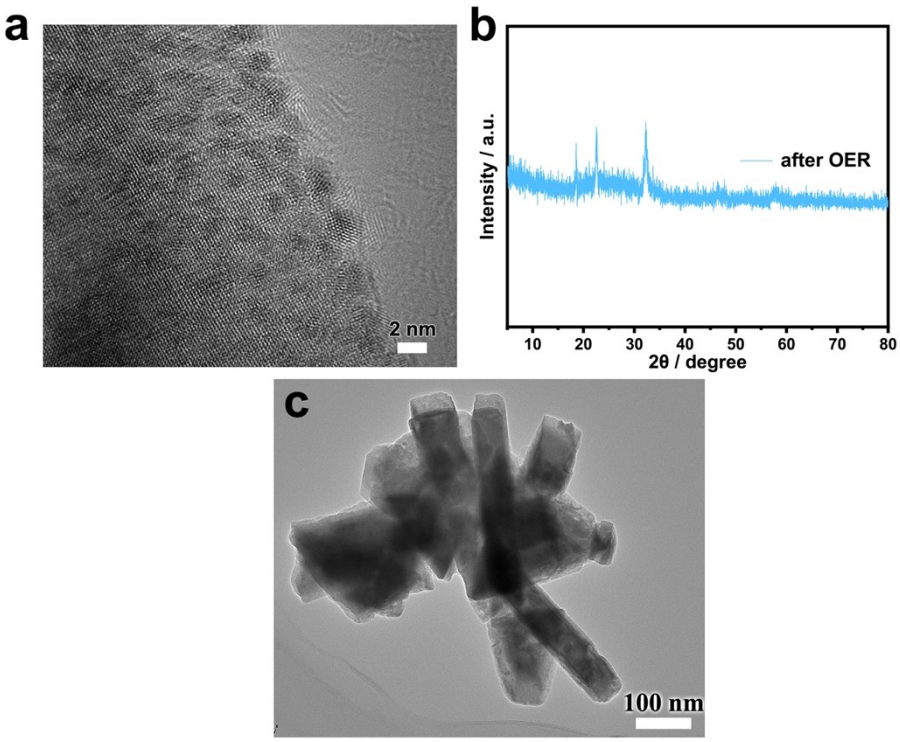

Fig. S7. (a) HRTEM images, (b) XRD and (c) TE images of $Sr_2CaRu_2IrO_9$ after OER.

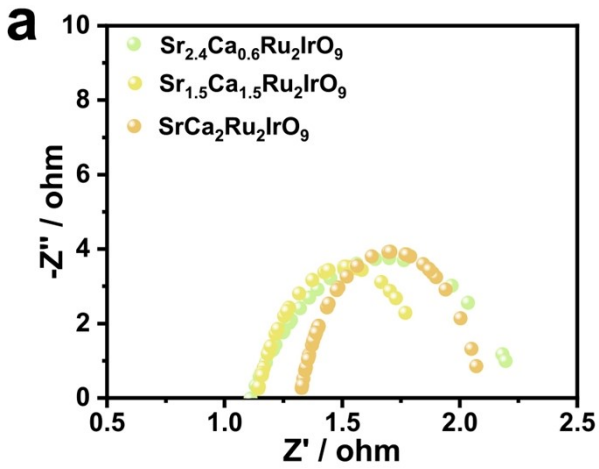

Fig. S8. EIS Nyquist plots of $Sr_xCa_{1-x}Ru_2IrO_9$ with different Sr: Ca atomic ratios.

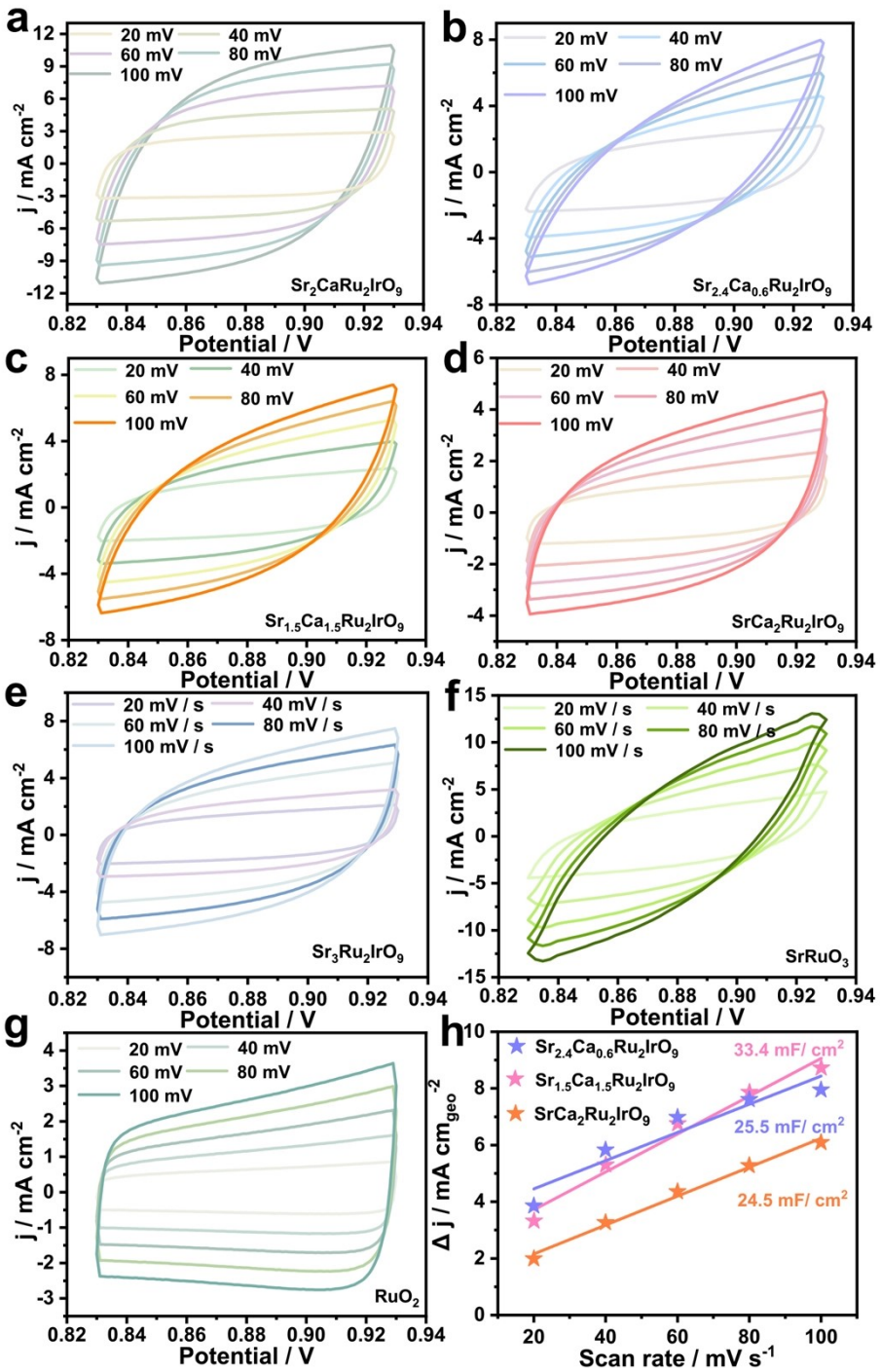

Fig. S9. (a-g) CV curve of $SrRuO_3$, $Sr_3Ru_2IrO_9$, RuO_2 and $Sr_xCa_{1-x}Ru_2IrO_9$ with different Sr: Ca atomic ratios. (h) Double-layer capacitance of $Sr_{2.4}Ca_{0.6}Ru_2IrO_9$, $Sr_{1.5}Ca_{1.5}Ru_2IrO_9$ and $SrCa_2Ru_2IrO_9$.

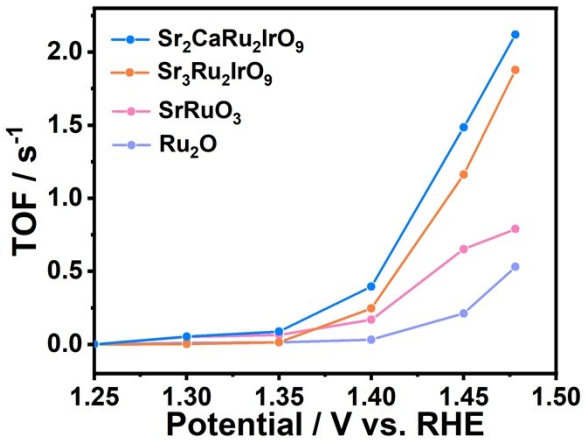

Fig. S10. TOF values of $Sr_2CaRu_2IrO_9$, $Sr_3Ru_2IrO_9$, $SrRuO_3$ and commercial RuO_2.

References

[1] G. Kresse, J. Hafner, Ab Initiomolecular Dynamics for Liquid Metals, *Phys. Rev. B* , **1993,** 47, 558-561.

[2] G. Kresse, J. Hafner, Ab Initiomolecular-Dynamics Simulation of the Liquid-Metal-Amorphous-Semiconductor Transition in Germanium, *Phys. Rev. B*, **1994,** 49, 14251-14269.

[3] J. P. Perdew, K. Burke, M. Ernzerhof, Generalized Gradient Approximation Made Simple. *Phys. Rev. Lett.*, **1996**, 77, 3865-3868.

[4] G. Kresse, D. Joubert, From Ultrasoft Pseudopotentials to the Projector Augmented-Wave Method. *Phys. Rev. B*, **1999**, 59, 1758-1775.

[5] P. E. Blöchl, Projector Augmented-Wave Method, *Phys. Rev. B*, **1994,** 50, 17953-17979.

[6] Nørskov JK, Rossmeisl J, Logadottir A, Lindqvist L, Kitchin JR, Bligaard T, Jonsson H. Origin of the overpotential for oxygen reduction at a fuel-cell cathode. *J. Phys. Chem. B*, **2004**, 108, 46, 17886–17892.

[7] Bendavid LI, Carter EA. CO_2 Adsorption on Cu_2O(111): A DFT+U and DFT-D Study, *J. Phys. Chem. C*, **2013**, 117, 49, 26048–26059.